A blended global snow product using visible, passive microwave and scatterometer satellite data

JAMES L. FOSTER*[1], DOROTHY K. HALL[1], JOHN B. EYLANDER[2], GEORGE A. RIGGS[3],
SON V. NGHIEM[4], MARCO TEDESCO[5], EDWARD KIM[1], PAUL M. MONTESANO[3],
RICHARD E.J. KELLY[6], KIMBERLY A. CASEY[7], AND BHASKAR CHOUDHURY[1]

1 NASA/GSFC, Hydrospheric and Biospheric Sciences Laboratory, Greenbelt, MD, USA
2 HQ AF Weather Agency,106 Peacekeeper Dr., Suite 2N3, Offutt AFB, NE, USA
3 Science Systems and Applications, LANHAM, MD, USA
4 jet propulsion laboratory, California Institute of Technology,
4800 Oak Grove Drive, Pasadena, CA, USA
5 City University of New York, NY, NY, USA
6 Waterloo University, Geography Department, Waterloo, Ontario, Canada
7 Wylie Laboratories Inc., McLean, VA, USA

Correspondence *James L. Foster Email: James.L.Foster@nasa.gov

Abstract

A joint U.S. Air Force/NASA blended, global snow product that utilizes Earth Observation System (EOS) Moderate Resolution Imaging Spectroradiometer (MODIS), Advanced Microwave Scanning Radiometer for EOS (AMSR-E) and QuikSCAT (Quick Scatterometer) (QSCAT) data has been developed. Existing snow products derived from these sensors have been blended into a single, global, daily, user-friendly product by employing a newly-developed Air Force Weather Agency (AFWA)/ National Aeronautics and Space Administration (NASA) Snow Algorithm (ANSA). This initial blended-snow product uses minimal modeling to expeditiously yield improved snow products, which include snow cover extent, fractional snow cover, snow water equivalent (SWE), onset of snowmelt, and identification of actively melting snow cover. The blended snow products are currently 25-km resolution. These products are validated with data from the lower Great Lakes region of the U.S., from Colorado during the Cold Lands Processes Experiment (CLPX), and from Finland. The AMSR-E product is especially useful in detecting snow through clouds; however, passive microwave data miss snow in those regions where the snow cover is thin, along the margins of the continental snowline, and on the lee side of the Rocky Mountains, for instance. In these regions, the MODIS product can map shallow snow cover under cloud-free conditions. The confidence for mapping snow cover extent is greater with the MODIS product than with the microwave product when cloud-free MODIS observations are available. Therefore, the MODIS product is used as the default for detecting snow cover. The passive microwave product is used as the default only in those areas where MODIS data are not applicable due to the presence of clouds and darkness. The AMSR-E snow product is used in association with the difference between ascending and descending satellite passes or Diurnal Amplitude Variations (DAV) to detect the onset of melt, and a QSCAT product will be used to map areas of snow that are actively melting.

1. Introduction

Seasonal snow cover is a key component of the Earth's energy balance and a key storage mechanism for water. In many areas of the world, people rely on snowmelt runoff for their water resources. For example, melting snow contributes upwards of 70% of the total annual water supply in the western USA, and in India, Pakistan, Afghanistan, and Nepal. Snow and ice melt from the Hindu Kush and Himalayan ranges is a vital resource for nearly a billion people (Foster et al., 2007). The ability to characterize snow storage more accurately at the drainage basin scale is crucial for improved water resource management. Snow-water equivalent (SWE), snow extent, and melt onset are important parameters for climate modeling and for the initialization of forecasts at daily and seasonal time scales. Snowmelt data are needed in hydrological models to improve flood control and irrigation management. In addition, knowledge of snowpack ripening is essential for natural-hazard applications such as flood prediction. Data on snow depth and snowmelt are important to assess trafficability for military tactical operations.

The Air Force Weather Agency's (AFWA) snow depth analysis model (SNODEP) is responsible for generating daily global snow depth and snow age analyses. SNODEP is

used extensively by AFWA and external customers. The operational SNODEP uses snow depth reports from synoptic observations combined with Defense Meteorological Satellite Program (DMSP) Special Sensor Microwave/Imager (SSM/I) passive microwave data and climatology to generate a global analysis of snow depth and snow age. The paucity of synoptic snow depth observations presents a unique challenge to accurately represent snow information in locations where regular meteorological observations are unavailable due to a lack of hydrometeorological monitoring infrastructure. Recent advances in remote sensing have led to further algorithm developments to improve the measurement accuracy of snow depths from space using the Advanced Microwave Scanning Radiometer for the Earth Observing System for EOS (AMSR-E) sensor (Kelly, in press). Additionally, algorithms using visible, near infrared and infrared radiances from the Moderate Resolution Imaging Spectroradiometer (MODIS) instrument on board the National Aeronautics and Space Administration (NASA) Aqua and Terra satellites produce binary and fractional snow cover at spatial resolutions up to 500 m. The algorithms developed for AMSR-E and MODIS data are potentially applicable to other current operational satellite missions, including NOAA (National Oceanic and Atmospheric Administraion) polar orbiting satellites, MeteoSat 8/9 satellites, and the planned National Polar-Orbiting Environmental Satellite System (NPOESS) Visible Infrared Imager Radiometer Suite (VIIRS). NASA is actively working with AFWA to improve the SNODEP model to take advantage of new techniques using remotely sensed measurements blended from AMSR-E, MODIS and QSCAT data products.

The snow algorithm blended satellite data is referred to as the Air Force Weather Agency/NASA Snow Algorithm (ANSA). Because snow cover extent is identified better at visible wavelengths than at microwave wavelengths, cloud-free MODIS observations are used as the default. The microwave-derived snow cover will be used only in those areas where the MODIS results are limited by clouds and darkness.

Our blended-snow product is automated and is thus amenable to the production of future climate-data records (CDRs) or Earth Science Data Records (ESDRs), following necessary re-processing. Specifically, this comprehensive blended-snow product includes SWE from the AMSR-E product (Kelly et al., 2003; Kelly and Foster, in press), snow extent with fractional snow cover from an existing MODIS product (Hall et al., 2002; Hall and Riggs, 2007b), and snowmelt from AMSR-E and QSCAT (Nghiem and Tsai, 2001).

Though snow-cover extent and snow albedo are currently available from various instruments including the MODIS (Hall and Riggs, 2007b), and SWE is available from the AMSR-E (Kelly et al., 2003; Foster et al., 2005); the onset of melt and snowpack melting are currently unavailable as standard products. Nonetheless, QSCAT scatterometer data are highly suited to assessing area of active snowmelt (Nghiem and Tsai, 2001) and QSCAT data can be complemented with AMSR-E data for melt-onset detection. There are several advantages of using active and passive microwave observations together for snow monitoring. The instrument spatial resolutions are similar (~20-25km); the incidence angles are comparable (QSCAT: 46º for H and 54º for V channel, SSM/I/AMSR-E: ~53º); both instruments have a wide swath (QSCAT 1800 km, SSM/I 1400 km), and both have

sun-synchronous polar orbits allowing frequent coverage across the immense extension of cold land regions.

It is not straightforward for the snow research and application communities to utilize all of the above products separately because of disparities in spatial coverage, file types, footprint size, geographic grid, and the coverage frequency. The blended product that we are developing will provide the suite of necessary snow outputs (snow extent, SWE, fractional snow cover, snowpack ripening, onset of snowmelt, and actively melting areas) in a single user-friendly global product.

The ANSA blended-snow product will begin with the first combined MODIS/AMSR-E data from the Aqua satellite (June 2002) and continue through the present. It is an all-weather product with snow mapped using visible, near-IR and IR (VNIR) MODIS data for daylight clear-sky conditions, and by AMSR-E and QSCAT data when clouds and darkness obscure the surface. Melt onset at the global scale will be derived by using both QSCAT and AMSR-E data. By blending products, we complement their capabilities and reduce the uncertainty in each separate product.

2. Data sets

2.1 MODIS

MODIS data have been used since early 2000 to produce validated, daily, global snow maps in an automated environment (http://modis-snow-ice.gsfc.nasa.gov). These maps, available at a variety of spatial resolutions – 500 m, 0.05° and 0.25° – provide snow extent, fractional-snow cover (FSC) and snow albedo (Hall et al., 2002; Klein and Stroeve, 2002; Salomonson and Appel, 2004; Riggs et al., 2006; Hall and Riggs, 2007b) in both a sinusoidal projection and a latitude/longitude grid known as the climate-modeling grid (CMG). Validation activities for snow extent and FSC have been conducted by the data-product developers and also by other investigators (Hall and Riggs, 2007b).

There is a long history of using a normalized difference of visible and near infrared bands to map snow (e.g., Crane and Anderson, 1984; Dozier, 1989; Hall et al., 2002). MODIS snow algorithms have been developed using the MODIS bands listed in Table 1. Inputs to the MODIS standard snow products include the MODIS cloud mask, land/water mask, geolocation product, radiance products and land cover. These algorithms were modified from heritage algorithms that were successfully used on earlier sensors and are described in detail in the MODIS Snow and User Guide (Riggs et al., 2006).

The MODIS snow products provide global, daily coverage (Table 2). Swath and daily products are available at 500-m resolution, while the CMG products are provided at 0.05° resolution (~5.6-km resolution at the Equator). FSC or percent snow cover is available in the CMG and in the 500-m resolution products. Because cloud cover often precludes the acquisition of snow cover from VNIR sensors, 8-day composite products that minimize cloud obscuration complement the daily products. Quality-assessment (QA) information is included in all products.

The automated MODIS snow-mapping algorithm uses at-satellite reflectances in MODIS bands 4 (0.545-0.565 μm) and 6 (1.628-1.652 μm) to calculate NDSI (normalized-difference snow index) defined as

$$\text{NDSI} = (\text{band 4} - \text{band 6})/(\text{band 4} + \text{band 6}) \quad [\mathbf{1}]$$

A pixel in a non-densely-forested region will be mapped as snow if the NDSI is ≥0.4 and reflectance in MODIS band 2 (0.841-0.876 μm) and MODIS band 4 (0.545-0.565 μm) are ≥10%. However, if the MODIS band 4 or band 2 reflectance is <10%, then the pixel will not be mapped as snow even if the other criteria are met. This threshold test prevents pixels containing very dark targets such as black spruce forests, or clear water bodies from being mapped as snow because very low reflectances cause the denominator in the NDSI to be quite small, and only small increases in the visible wavelengths are required to make the NDSI value high enough to misclassify a pixel as snow.

Changes that occur in the spectra of a forest stand as it becomes snow covered can be exploited to map snow cover in forests (Klein et al., 1998). The primary change in reflectance occurs in the visible wavelengths as snow has a much higher visible reflectance than that of soil, leaves or bark. A fundamental change that snow cover causes in the spectral response of a forest, which can be used in a global algorithm, is that the reflectance in the visible will often increase with respect to the near-infrared reflectance. This behaviour is captured in the normalized-difference vegetation index (NDVI), as the presence of snow cover will tend to lower the NDVI. The NDVI (calculated using MODIS bands 1 and 2) and NDSI are used together to improve snow mapping in dense forests. If the NDVI and NDSI values of a pixel lie in a triangular polygon region of NDVI to NDSI space, then the pixel may be mapped as snow even if the NDSI is <0.4 (Klein et al., 1998).

The introduction of a 'thermal mask' has improved the snow-mapping result by eliminating much of the spurious snow cover that was found in many parts of the globe in the earlier MODIS snow maps. Some causes of the spurious snow cover are confusion with cloud cover, aerosol effects, geologic surface features and snow/sand confusion on coastlines. The thermal mask has greatly reduced errors of commission. Using MODIS IR bands 31 and 32, a split-window technique (Key et al., 1997), is used to estimate ground temperature. If the temperature of a pixel is higher than 283K, then the pixel will not be mapped as snow even if all of the other criteria are met.

An Aqua-specific version of the Level-2 snow algorithm was developed in response to MODIS instrument performance issues (see Riggs et al., 2006). Because most of the Aqua MODIS band 6 detectors are non-functional, the Aqua-specific version of the snow-mapping algorithm uses MODIS band 7 instead of band 6 for the calculation of NDSI. Snow reflectance is similar in both bands 6 and 7 so the difference in snow reflectance in the NIR relative to the VIS is similar and the NDSI criterion can be applied using band 7 in the ratio.

2.2 AMSR-E dataset and passive microwave radiometry

Passive microwave-derived methods to estimate regional to global snow depth or SWE use frequent and wide-swath-coverage observations from sensors on board several different satellites. There is a heritage of nearly 30 years of global-daily observations from such instruments (Chang et al., 1976 and 1987; Walker and Goodison, 2000). From November 1978 to the present, the SMMR instrument on the Nimbus-7 satellite and the SSM/I on the DMSP series of satellites have acquired passive microwave data that can be used to estimate SWE. The SMMR instrument failed in 1987, the year the first SSM/I sensor was placed in orbit. The AMSR-E sensor, launched in 2002 on board the Aqua satellite, is the most recent addition to the passive microwave suite of instruments. AMSR-E snow products (Kelly et al., 2003, Kelly, in press) are archived and distributed through the National Snow and Ice Data Center, and are available in the Equal Area SSM/I Earth Grid (EASE-grid) projection (at a 25 km x 25 km pixel scale).

Passive microwave snow data products are available globally, every day. The data are projected into ½º latitude by ½º longitude grid cells uniformly subdividing a polar stereographic map according to the geographic coordinates of the center of the field of view of the radiometers. Overlapping data in cells from separate orbits are averaged to give a single brightness temperature, assumed to be located at the center of the cell (Armstrong and Brodzik, 1995; Chang and Rango, 2000).

An extensive body of literature describes the ability of passive-microwave instruments to estimate snow extent, SWE and melt onset (e.g., Chang et al., 1987). There is also a growing set of literature describing systematic errors and uncertainties in SWE retrievals using passive-microwave data (Foster et al., 2005).

Microwave emission from a snow layer over a ground medium consists of contributions from the snow and from the underlying ground. Both contributions are governed by the transmission and reflection properties of the air-snow and snow-ground boundaries, and by the absorption and scattering properties of the snow layers (Chang et al., 1976; Matzler and Standley, 2000). Snow crystals scatter part of the cold sky radiation, which reduces the upwelling radiation measured with a radiometer (Schmugge, 1980). The deeper or more compact the snowpack, the more snow crystals are available to scatter the upwelling microwave energy. It is this interaction property that is used to estimate snow mass (Foster et al., 2005).

Meltwater in the snowpack can raise the microwave brightness temperature, especially at frequencies above about 30 GHz, since water droplets emit rather than scatter microwave radiation. While SWE is difficult to extract under these conditions, it is possible to use this characteristic to infer information on snowmelt status (Walker and Goodison, 1993). In order to minimize the effect of these conditions on SWE estimates, only nighttime data have been used in this study. This alleviates snowmelt effects due to refrozen or partially refrozen snow at lower nighttime temperatures (Derksen at al., 2000; Foster et al., 2005).

AMSR-E is fitted with 18.7 GHz and 36.5 GHz sensors (Table 3). Note that the SSMR, SSM/I and AMSR-E instrument characteristics at these frequencies are similar.

To derive SWE from space-borne sensors, brightness temperature differences between the 18.7 and 36.5 GHz channels are multiplied by a coefficient related to the average snow grain size to derive SWE (Chang at al., 1987) as follows

$$SWE = C\,(T_{18} - T_{37})\ \text{mm} \qquad [\mathbf{2}]$$

Where SWE is snow water equivalent in mm, C is the grain-size coefficient and T_{18} (T_{19}) and T_{37} are the brightness temperatures at the 18 (19) GHz and 37 GHz vertical polarizations, respectively. To determine snow depth, the quantity derived from [**2]** can be multiplied by the approximate density of mid winter snowpacks in the range of 200-400 kg^{-3}. C is based on the particular snow class or zone of interest. It has been determined that the average crystal sizes are larger (smaller coefficient) in regions where temperature and vapor gradients are quite large, such as tundra areas. In contrast, in maritime and alpine areas the crystals sizes are generally smaller (larger coefficient) than those found in prairie or tundra locations. Further information of properties on different snow classes was reported by Sturm et al. (1995) and Foster et al. (2005).

The current SWE algorithm is an evolution of the original SWE algorithm based on [2] (Chang et al., 1987). The current algorithm utilizes several more channels on the AMSR-E instrument, especially the 10 GHz channel. Since there are many more snow-depth measuring sites in the Northern Hemisphere for testing, the algorithm was calibrated for snow depth and a snow density data set, based on average Canadian (Brown and Braaten, 1998) and Russian (Krenke, 1998) snow density records for the months of January through March. The algorithm, adopted in September 2005, is currently operational (version B07) and results are distributed by the National Snow and Ice Data Center (NSIDC).

Version B07 is derived as follows. AMSR-E brightness temperatures are acquired and used at native channel resolution, with the exception of the 89 GHz channel, which is re-sampled to the 37 GHz channel resolution. Thresholds are then checked to ensure cold snow conditions are present at 37 GHz (Tb_{36H}<245K and Tb_{36V}<255K). If this condition is met, then snow is identified for retrieval of snow depth in the class of shallow-medium depth. Otherwise, the pixel is classified as snow free.

If Tb_{10V}-Tb_{36V} > 0 K or Tb_{10H}-Tb_{36H} > 0 K, then medium to deep snow is assumed to be present. If Tb_{10V}-Tb_{36V} ≤ 0 K and Tb_{10H}-Tb_{36H} ≤ 0 K, then snow presence is possible, but it is likely to be shallow snow if Tb_{89V} ≤ 255 K, Tb_{89H} ≤ 265 K, Tb_{23V}-Tb_{89V} > 0 K, Tb_{23H}-Tb_{89H} > 0 K, and T_{snow_K} < 267 K[1]. If shallow snow is in fact observed, snow depth is estimated as 5.0 cm. In the current algorithm, brightness temperatures at 89 GHz are used more effectively.

For the retrieval of snow depth, the following general procedure is followed:

$$SD = ff(SD_f) + (1\text{-}ff)x(SD_o) \qquad [\mathbf{3}]$$

[1] T_{snowK} is calculated from the expression derived for snow in Kelly et al. (2003)

where SD is the total sample snow depth, SD_f is the snow depth from the forest component of the instantaneous field of view (IFOV) and SD_o is the snow depth from non-forested component of the IFOV. The quantity *ff* is the forest fraction (where 1.0 = 100% forest fraction and 0.0 = 0% forest fraction).

$$SD_f\,[cm] = 1/\log_{10}(pol_{36}) \times (Tb_{18V}-Tb_{36V})/(1-fd \times 0.6) \quad [\mathbf{4}]$$

$$SD_o\,[cm] = [1/\log_{10}(pol_{36}) \times (Tb_{10V}-Tb_{36V})] + [1/\log_{10}(pol_{18}) \times (Tb_{10v}-Tb_{18V})] \quad [\mathbf{5}]$$

where *fd* is forest high spatial resolution (500m) density (g cm^{-3}) from the University of Maryland Vegetation Continuous Fields (VCF) data product (Hansen et al. 2003), circularly smoothed at 15-km diameter and re-gridded globally in 1-km grid cells. In [4] and [5], $pol_{36} = Tb_{36V}-Tb_{36H}$ (NB if $pol_{36} < 1.1$ then $pol_{36}=1.1$ to ensure $\log(pol_{36}) > 0$), and $pol_{18} = Tb_{18V}-Tb_{18H}$ (NB if $pol_{18} < 1.1$ then $pol_{18}=1.1$ to ensure $\log(pol_{18}) > 0$). Note the use of the difference between the 18 and 36 GHz channels to maximize spatial resolution in forested areas, and the use of 10V-36V (increased dynamic range) and 10V-18V for deep snow, also that *fd* is scaled (0.6) through optimization of validation data. For more about this, see Kelly (in press).

To convert SD to SWE, a density map in EASE-grid projection was produced by mapping the mean January through March density measurements from data sets of Brown and Braaten (1998) and Krenke (2004) to the Sturm et al. (1995) seasonal snow classification map. Within each snow class, the average *in* situ density was computed and this value is assigned to all pixels in the same snow class. Therefore, an average density is available for each of the six snow classes delineated by Sturm et al. (1995). The final SWE is estimated using a snow density data set such that for any snow pixel

$$SWE\,[mm] = SD\,(cm) \times density\,(g\ cm^{-3}) \times 10.0 \quad [\mathbf{6}]$$

2.3 QSCAT data set and active microwave scatterometry

The sensitivity of spaceborne scatterometer data to snow parameters has been gaining more attention in recent years (e.g., Nghiem and Tsai 2001; Kimball et al. 2001; Hallikainen et al., 2004). Nghiem and Tsai (2001) indicate the potential of the NASA scatterometer (NSCAT) data for applications to remote sensing of snow at the global scale by showing that Ku-band (14 GHz) backscatter is sensitive to snow properties and that onset of snowmelt can be detected with NSCAT data. Moreover, the diurnal backscatter change method was developed to detect and map snowmelt areas using QSCAT data (Nghiem et al., 2001). Preliminary results show that the detection of snow cover can be improved when both active and passive data are used together, rather than when each is used alone (e.g., Nghiem et al., 2005).

At the wavelength of 2.2 cm (Ku-band 13.4 GHz), QSCAT backscatter is highly sensitive to snow wetness. In wet snow, liquid water (no salinity) has an imaginary part of about 19 000 times larger than that of dry ice. Thus, a small amount of wetness can significantly change

the imaginary part of the snow effective permittivity, and consequently decrease the backscatter.

With the wide swath (1800-km) of QSCAT, is the coverage frequency is two times per day across most cold land regions, once in the morning and once in the afternoon because of the sun synchronous orbit. Due to diurnal cycling of air temperature, satellite measurements are made at cold conditions in the early morning and warm condition in the late afternoon snow image. Such diurnal data enable the use the amount of backscatter cycling in the identification of the stage of the snowmelt transition.

Here, we use the diurnal difference method first developed by Nghiem et al. (2001) to determine snowmelt. A diurnal difference is defined as the relative backscatter difference between morning and afternoon measurements. We co-locate the data from the early morning (t_a) in an ascending orbit pass and late afternoon (t_p) in a descending pass for each day. The diurnal backscatter change is defined as the backscatter difference in the decibel (dB) domain as

$$\Delta\sigma_{VV} = \sigma_{VV}(t_p) - \sigma_{VV}(t_a) \qquad [7]$$

where σ_{VV} is the vertical-polarization backscatter and all quantities are in dB. A backscatter difference of 1.8 dB corresponds snow containing a volumetric wetness of 1%, which is used to identify snowmelt (Nghiem et al., 2001). We adapt this algorithm for snowmelt detection on land. This algorithm has several advantages:

(1) Independent of the scatterometer long-term gain drift,
(2) Independent of the cross-calibration between QSCAT and future satellite scatterometers,
(3) Independent of absolute backscatter from different snow classes and snow conditions,
(4) Detection of both snow melt and refreezing,
(5) Daily coverage over most cold land regions.

3. Snow extent and SWE from the blended product

The current operational AFWA SNODEP model lacks the capability to measure global snow depths and SWE accurately due to the sparse nature of synoptic observations compounded by a lack of remotely sensed observations used within the model infrastructure. Failure to address these deficiencies results in continued poor representation of snow depth analysis, which is used by the AFWA Land Information System (LIS) to represent the surface water and energy budgets, and by the Weather Research and Forecasting (WRF) models to predict the surface water and energy budget. The SNODEP model also supports current operational customers in the National Intelligence Community (NIC) and U.S. Army. Improvements to the SNODEP model are also required to improve the AFWA Cloud Depiction and Forecast System version II (CDFSII) global cloud analysis. Finally, improving SNODEP will be necessary for AFWA NPOESS preparation,

with AFWA unable to use NPOESS VIIRS or replacement Microware Imager/Sounder datasets within its land surface modeling capability.

Figures 1-3 show Northern Hemisphere ANSA maps for January, February and April 2007, respectively. Twenty one separate categories are presented, 15 of which show snow from either or both the MODIS and AMSR-E products. The deeper blue colour shows snow cover from both products. Red portrays areas where MODIS detects snow and AMSR-E does not – especially evident near the border of the continental snowline where snow depths are typically shallow (Figure 3). On this rendition, the yellow colour represents snow observed by AMSR-E but not by MODIS. Gray areas are snow free according to both products, and black indicates lands with snow cover detected by AMSR-E and cloud cover identified in the MODIS cloud mask. The bottom half of each figure shows only the blended snow cover extent.

Notice the amount of cloud cover from MODIS (black) over both North America and Eurasia. More than a third of the northern portions of both continents is obscured by clouds during many winter months. However, the MODIS snow product shows more excessive clouds than are really present due to the conservative nature of the cloud mask (Ackerman et al., 2002) that is used as an input to the snow product. As mentioned previously, the PM product is especially useful in detecting snow through clouds. Although, with PM approaches, there is difficulty in observing snow in those regions where the snow cover is rather thin (<5 cm), along the margins of the continental snow line and on the lee side of the Rocky Mountains, for instance. In these areas, MODIS can easily map shallow snow cover as long as it is not ephemeral and is at least ~2 cm deep.

The extensive turquoise area on the January image (Figure 1) over northern Siberia, Alaska and the Canadian Archipelago results from polar darkness. In mid January, the Sun is not yet above the horizon in far northern latitudes.

The areas in yellow, where AMSR-E appears to map snow but MODIS does not, are primarily located on very high and dry plateaus, such as the Tibet Plateau in western China. This massive plateau, though almost always below freezing during the winter months, is generally snow free because the atmosphere is so dry. The AMSR-E product overestimates snow extent there because the passive microwave algorithm is detecting a very cold surface (low brightness temperatures), and therefore this region is misclassified as snow covered.

Figure 4 shows a blended MODIS and an AMSR-E map for 27 January 2007. Here, the AMSR-E swath gaps, visible on Figures 1-3, have been filled. Current-day AMSR-E swath gaps are filled with SWE data from the previous day. The SWE gap filling is done prior to application of the ANSA sensor blending rules. Swath gap discontinuities are eliminated and snow cover is mapped using both instruments.

A technique is being developed to fill observational gaps caused by cloud cover and orbital gaps in the ANSA snow product. Orbital gaps in the AMSR-E SWE data product that occur on the current day will be filled with AMSR-E observations from the previous day. These orbital gaps change location each day in a progressive movement pattern such that they

rarely overlap between days. Thus, using the previous day to fill current day orbital gaps allows us to generate gap-free daily SWE maps for the ANSA snow product.

AMSR-E orbital gaps extend from the equator to about 50º latitude; they narrow as they extend northward. The gaps impact SWE mapping by preventing the complete coverage of snow covered regions. In many cases, thousands of km^2 of the surface are affected. Using data from the previous day gives complete daily coverage and provides continuity in SWE mapping with little loss of 'real time' data, except in cases where snow cover changes rapidly between days in areas where gaps are present.

Daily observational coverage gaps caused by cloud cover in the MOD10C1 snow extent maps used in the ANSA product are filled using the last 'clear' observation of the surface. If there is cloud cover in a grid cell on the current day, then the last 'clear' observation for that grid cell is retained an used as the 'observation' for the current day. This technique gives a nearly cloud-free observation map of snow cover extent after 5-7 consecutive days. However, snow events occurring under cloud cover are not observable until the next clear-sky condition. Clearing skies may occur immediately after a snow storm or perhaps days later, thus the appearance of snow cover using our approach may be observed one or more days after the event. Persistence of cloud cover since the last clear observation of the surface causes a deterioration of the accuracy of the gap-filled snow map with time. A cloud-persistence map, which is the count of days since the last clear view observation, will be provided with the gap-filled snow map. The purpose of the cloud-persistence map is to aid the analyst, when using the gap filled snow map, in gauging the confidence associated with this product. For example, if the cloud cover has existed for a day or two, confidence and accuracy of the gap-filled product may be considered as high, but if the cloud cover has persisted for five or six days, then the confidence level would be considered as low. Various techniques to improve the MODIS gap-filled product may be employed and are discussed by Hall et al. (in preparation – should be submitted in November 2008).

4. ASSESSING SNOWMELT

4.1 Snowmelt and snow accumulation from QSCAT data

Ku band scatterometer (QSCAT) data are used to obtain snowmelt area based on the diurnal difference method described above. To illustrate the capability of QSCAT to monitor snowmelt daily on a hemispheric scale, we present snowmelt results over the Northern Hemisphere in Figure 5 for a series of snowmelt maps in April 2001. The series of continental snowmelt patterns shows the northward migration of the melting process as expected: melt occurred at lower latitudes first and later at higher latitudes interlaced with periods of refreezing and melt recurrences. An interesting observation is that the snowmelt regime appears as a coherent extensive longitudinal stretch as seen, for example, by the red band across the North American continent on 18 April 2001 (center panel in Figure 5). Note that the northern extent of this snowmelt band approximately occurs along the Canadian Shield from the west of Hudson Bay to the east of Yukon Territory. The temporal evolution of large-scale snowmelt is not abrupt and it exhibits periods of melting and refreezing as the snowmelt advances northward. In fact, an animation of the daily

time-series maps of snowmelt reveals oscillations in snowmelt patterns over the continental scale.

Ku-band backscatter is also sensitive to snow accumulation. Change in backscatter as a function of snow depth at Ivotuk (68.5°N, 155.8°W) in Alaska is shown in Figure 6 for snow seasons in 1999, 2000, and 2001. Regression analysis shows that the slope of the snow depth change versus backscatter change is similar in different years. Note the similarity in the slope of the curves for different years. The bias in absolute backscatter in each year is dependent on the condition of the landscape in different years (different number of bushes, different characteristics in the initial snow cover layer at the beginning of the snow season, etc.). This result indicates that snow depth at Ivotuk can be retrieved consistently based on the backscatter change from the initial backscatter level, which is determined by the minimum background backscatter of the frozen landscape at the beginning of snow season. The root-mean-squared (RMS) errors for snow depth retrieval can be between 4 to 6.6 cm, or 1.3 to 2.2 cm in SWE.

4.2 Snowmelt from AMSR-E data (snowmelt onset)

Passive microwave radiometry is utilized to assess the onset of snowmelt. Melt onset is detected when the AMSR-E brightness temperature at 19.35 GHz (horizontal polarization) and the difference between ascending and descending passes using the Diurnal Amplitude Variations (DAV) developed by Ramage and Isacks (2002) and applied to seasonal non-glacier snow accumulation (Ramage et al., 2007). In order to account for melting that might persist during the night, we use the rule that snow is melting when both ascending and descending brightness temperatures are greater than the threshold value. The main hypothesis is that histograms of brightness temperatures measured during both dry and wet snow conditions can be modeled by means of a bimodal distribution, with the left-normal distribution (LND) being representative of dry snow conditions and the right-normal distribution (RND) representative of wet snow conditions.

Threshold values used within the DAV algorithm for different frequencies are defined as

$$T_{b37v} > 242 \text{ K} \quad \text{AMSR-E}$$
$$\text{DAV} = \text{abs}(\text{Tb ascending} - \text{Tb descending}) \; 10 \text{ K} \qquad [\mathbf{8}]$$

and

$$T_{b19h} > 243 \text{ K} \quad \text{AMSR-E}$$
$$\text{DAV} = \text{abs}(\text{Tb ascending} - \text{Tb descending}) \; 24 \text{ K} \qquad [\mathbf{9}]$$

Thus, wet snow can be detected according to the condition that measured brightness temperature belongs to the RND and that the difference between nighttime and daytime measurements is greater than a threshold value. This last condition assures us that the change in brightness temperatures is related to the appearance of liquid water (because of the abrupt and sudden change in brightness temperature) instead of other factors. The current version of the algorithm uses the same threshold over all areas. However, an updated version has been developed, in which the threshold on both brightness temperature and DAV is computed for each pixel by minimizing (maximizing) the probability that a measured brightness temperature belongs to the set of dry (wet) snow pixels. This algorithm is undergoing testing.

In order to consider only those areas covered by snow, microwave and visible data are re-projected into the same projection with a resolution of 0.25º and co-registered (Figure 7). Only those pixels classified by MODIS as snow are shown.

Results obtained over the Arctic are shown in Figure 8 -- for the period October 2004 – May 2005. From this figure, we see that the cumulative number of melting days between February and April 2003 ranges from 2 to 16 days. The areas showing the highest number of cumulative melting days includes Scandinavia, the Great Lakes region, and northwestern Canada.

Using AMSR-E and QSCAT data we have the capability of showing areas of dry snow (AMSR-E, 37 GHz), areas where melt is in the incipient stages (AMSR-E, 19 GHz horizontal channel), and areas where snow is actively melting (QSCAT, 13.4 GHz).

5. Evaluation of the blended snow product

5.1 Great Lakes and CLPX regions

The ANSA product for snow cover and has been evaluated for the Lower Great Lakes region during the winter of 2002-03 (Hall et al., 2007a). This study area is challenging for mapping snow cover using passive microwave (PM) sensors due to varied land cover and the frequency of lake-effect snows (deep and wet snowfalls). National Weather Service Co-Operative Observing Network (Co-op) stations were used as ground truth. An interpolation scheme was used to map snow cover on the ground from the station measurements for each day of the study period, though it was concluded that the interpolation technique did not represent the actual ground conditions adequately to permit evaluation of the new snow product in an absolute sense, largely because of the paucity of stations. Nevertheless, use of the ANSA product was found to improve the mapping of snow cover as compared to using either the MODIS or AMSR-E product, alone (Hall et al., 2007a).

Figure 9 shows the percentage of snow mapped using MODIS and AMSR-E data alone, and using the ANSA product for each day during the 2002-03 winter from 1 November 2002 through 31 March 2003, in comparison with a snow-cover map developed using kriging to interpolate the station data as discussed above. The contribution to the ANSA blended product is predominantly from MODIS in the early part of the snow season as seen in Figure 9, while the contribution from the AMSR-E becomes greater after mid-January. As the snow deepens during the winter, snow grain size increases and the temperatures become consistently colder, the ability of the passive-microwave sensors to map snow increases, and the agreement between the visible and passive-microwave maps improves as has been noted in previous work (see Basist et al., 1996; Armstrong and Brodzik, 2001).

The measurements derived from the NWS Co-op station data do not characterize the actual snow cover over the larger study area accurately over much of the 2002-03 winter. In addition, the density of the stations may not be adequate to conduct a validation study using ground measurements in a 25 km^2 cell. Chang et al. (2005) report that a density of 10 ground measurements in a 25 km^2 SSM/I or AMSR-E pixel is necessary in order to produce

a sampling error of 5 cm or better. That ground-truth or station density has not been achieved in this area.

The benefit of the ANSA blended-snow map is maximized when AMSR-E contributes where there is cloud cover and MODIS data are available to map snow at the edges of snow-covered areas. MODIS provides snow data under clear skies, and where there is shallow or wet snow – these types of snow cover may not be mapped using AMSR-E when used alone.

The primary limitation of the MODIS snow-cover maps is the inability of the MODIS to map snow through cloud cover. This study area is also very challenging for mapping snow cover using PM sensors due to the varied land cover and the frequency of lake-effect snows (deep and wet snowfalls). Especially in Wisconsin, the large number of small lakes further complicates the determination of SWE. The relatively coarse resolution of the AMSR-E product (25 km) is problematic, due to mixed-pixel effects, for mapping snow near the coasts of the Great Lakes where much of the lake-effect snow accumulates.

In an effort to address the issue of ground measurements density, we also explored the evaluation of the ANSA product of snow cover and snow water equivalent products using field observations from the NASA's Cold Land Processes Experiment-1 (CLPX-1). Specifically, we used observations from the February 2003 Intensive Observing Period (IOP-3) in Colorado.

CLPX-1 was a large-scale snow remote sensing field campaign in support of future NASA snow satellite missions. It included airborne and ground measurements for three 25×25 km^2 Meso-cell Study Areas (MSA) (Figure 10a). Of particular interest in the present context is the North Fork MSA where distributed ground measurements were collected within 25×25 km^2 area on February 22, 2003 (Figure 10b).

These in situ measurements were kriged to a 500-m grid to form an estimated ground-based SWE distribution (Tedesco et al., 2005). The mean SWE for the whole MSA was 18.9 mm with a standard deviation of 11.6 mm (because the snow cover was patchy). While the result on February 22 coincided with an AMSR-E swath, we can see that the 'true SWE' of 18.9 mm for that date (22 February 2003) was only 14% larger than the AMSR-E derived mean SWE for 21 and 23 February. While it is very difficult to draw definitive conclusions from such temporally sparse data, it is encouraging for this rare case of directly measured wide-area SWE. To expand validation of the ANSA product in space and time, future comparisons will necessarily involve airborne and interpolated station measurements of the 'true SWE.'

5.2 Finland

Satellite and in-situ data for snow extent and SWE are evaluated in Finland for the 2006-2007 snow season. Finnish Meteorological Institute (FMI) daily weather station data and Finnish Environment Institute (SYKE) bi-monthly snow course data are used as ground truth (Table 4). Early comparison results display positive agreement between the ANSA snow extent and SWE maps and in situ data, with discrepancies in accordance with known AMSR-E and MODIS snow mapping limitations (Figure 11) (Casey et al., in press).

From the FMI daily data, precipitation (rainfall) was mapped at the 9 field stations over the 2006-2007 snow season (Figure 11). Rainfall maximums occurred in October, December and May, with minimums in February and April. Although the degree of precipitation varied among the 9 field stations throughout the season, the seasonal pattern at each station is generally consistent among the 9 stations.

The comparison of AMSR-E derived SWE data corresponding with mid-month SWE snow course measurements at the Sodankylä Observatory are displayed on the AMSR-E SWE / SYKE snow course SWE histogram plot (Figure 11). The terrain category 'pine dominating forest' was selected as the snow course environment for the histogram comparison based on forest species description presented in (Hallikainen et al., 2000).

There is general agreement between the AMSR-E and snow course SWE measurements, with greater SWE measurement differences observed in February and March than the other months compared (November, December, January). As this was the first set of comparisons completed, as well as the only set of data currently available at one location throughout a large portion of the snow season, further SWE comparisons are needed. Nevertheless, known AMSR-E SWE mapping issues that may explain the deviations – including possible shallow snow cover, cold surfaces, or increased snow crystal grain size typical of the end of season snow

6. Conclusions and future work

The preliminary blended-snow product, ANSA, is an example of data fusion or blending, with minimal modeling in order to yield improved snow products, which include snow-cover extent, SWE, fractional snow cover, onset of snowmelt, and areas of snow cover that are actively melting. These maps will be in a user-friendly format, at 25-km resolution and have been evaluated thus far using data from the lower Great Lakes region, from the CLPX site in Colorado and from Finland.

Using AMSR-E and QSCAT data, we have the capability of delineating areas of dry snow (AMSR-E, 37 GHz), incipient melt using AMSR-E (19 GHz horizontal channel), and active-melt areas using QSCAT (13.4 GHz).

We will soon begin work on enhancing the resolution (currently 25 km) of the global daily snow cover and SWE products. We can improve the resolution, to 5 km since MODIS snow-cover products are already produced at ~5-km resolution (as well as at finer resolution), though the AMSR-E data will be sub-sampled to achieve the 5-km resolution. We will also incorporate an 89-GHz global snow detection and SWE algorithm into the blended product software. For QSCAT, the slice data with an improved resolution of 12 km can contribute to the improvement of the spatial resolution. We will continue to validate the snow products by using data from well maintained and reliable meteorological stations such as those found in Canada and selected World Meteorological Organization sites.

Acknowledgments

The research carried out at Goddard Space Flight Center and the Jet Propulsion Laboratory, California Institute of Technology was performed under an agreement with the Air Force Weather Agency and was also supported by NASA's Hydrology Program.

References

Ackerman, S.A., Strabala, K.I., Menzel, P.W.P., Frey, R.A., Moeller, C.C. and Gumley, L.E., 1998, Discriminating clear sky from clouds with MODIS. *JGR,* 103(D24): 32,141-32,157.

Armstrong, R.L. and Brodzik, M.J., 1995, An earth-gridded SSM/I data set for cryospheric studies and global change monitoring. *Advances in Space Research*, 10: 155-163.

Armstrong, R.L. and Brodzik, M.J., 2001, Recent northern hemisphere snow extent: a comparison of data derived from visible and microwave satellite sensors. *Geophysical Research Letters,* 28(19): 3673-3676.

Basist, A., Garrett, D., Ferraro, R., Grody, N. and Mitchell, K., 1996, A comparison between snow cover products derived from visible and microwave satellite observations. *Journal of Applied Meteorology,* 35(2): 163-177.

Casey, K.A., Kim, E., Hallikainen, M.T., Foster, J.L., Hall, D.K. and Riggs, G.A., in press, Validation of the AFWA-NASA blended snow-cover product in Finland, 2006 – 2007. In *Proceedings of the 65th Eastern Snow Conference,* Fairlee, Vt., 28 – 30 May 2008.

Chang, A.T.C., Gloersen, P., Schmugge, T., Wilheit, T., and Zwally, J., 1976, Microwave emission from snow and glacier ice. *Journal of Glaciology,* 16: 23-39.

Chang, A.T.C., Foster, J.L. and Hall, D.K., 1987, Nimbus-7 derived global snow cover parameters. *Annals of Glaciology*, 9:39-44.

Chang, A.T.C. and Rango, A., 2000, Algorithm Theoretical Basis Document (ATBD) for the AMSR-E Snow Water Equivalent Algorithm. NASA/GSFC, Nov. 2000.

Chang A.T.C., Kelly, R.E.J., Josberger, E.J., Armstrong, R.L. and Foster, J.L., 2005, Analysis of Gauge-measured and Passive Microwave Derived Snow Depth Variations of Snowfields. *Journal of Hydrometeorology,* 6:20-33.

Crane, R.G. and Anderson, M.R., 1984, Satellite discrimination of snow/cloud surfaces. International Journal of Remote Sensing, 5(1):213-223.

Derksen, C., LeDrew, E., Walker, A. and Goodison, B., 2000, The influence of sensor overpass time on passive microwave retrieval of snow cover parameters. Remote Sensing of Environment, 71 (3): 297-308.

Dozier, J., 1989, Spectral signature of alpine snow cover from the Landsat thematic mapper. Remote Sensing of Environment, 28:9-22.

Finnish Meteorological Institute. 2008a, 'Finland's Climate.' http://www.fmi.fi/weather/climate.html

Finnish Meteorological Institute. 2008b, 'A record mild December ended an unusually warm year 2006.' http://www.fmi.fi/weather/climate_13.html

Foster, J., Sun, C., Walker, J., Kelly, R., Chang, A., Dong, J., and Powell, H., 2005, Quantifying the uncertainty in passive microwave snow water equivalent observations. *Remote Sensing of the Environment*, 94:187-203.

Foster, J., Hall, D., Eylander, J., Kim, E., Riggs, G., Tedesco, M., Nghiem, S., Kelly, R., Choudhury, B., and Reichle, R., 2007, Blended Visible (MODIS), Passive Microwave (AMSR-E) and Scatterometer (QuikSCAT) Global Snow Products. In *Proceedings of the 64th Annual Eastern Snow Conference, St. Johns Newfoundland*, May 2007.

Foster, J., Hall, D., Eylander, J., Riggs, G., Nghiem, S., Tedesco, M., Kim, E., and Choudhury, B., 2008a, A new blended global snow product using visible, microwave and scatterometry satellite data. In *Proceedings of the 88th Annual Meeting of the A.M.S., New Orleans, Louisiana*, January, 2008.

Foster, J., Nghiem, S., Tedesco, M., Riggs, G., Hall, D., and Eylander, J., 2008b, A global snowmelt product visible, passive microwave and scatterometry satellite data. In *Proceedings of the XXI Congress of the ISPRSE, Beijing, China*, July, 2008.

Hall, D.K, Riggs, G.A., Salomonson, V.V., DiGirolamo, N.E. and Bayr, K.J., 2002, MODIS snow-cover products. *Remote Sensing of Environment* 83:181-194.

Hall, D.K., Riggs, G.A. and Salomonson, V.V., 2006, MODIS Snow and Sea Ice Products, 2006. In *Earth Science Satellite Remote Sensing - Volume I: Science and Instruments*, Qu, J.J., W. Gao, M. Kafatos, R.E. Murphy and V.V. Salomonson (eds.), Springer, New York, pp. 154 – 181.

Hall, D.K., Montesano, P., Foster, J.L., Riggs, G.A., Kelly, R.E.J. and Czajkowski, K., 2007a, Preliminary validation of the AFWA-NASA blended snow-cover product, *Proceedings of the 64th Eastern Snow Conference, St. John's, Newfoundland, Canada*, 28 May – 1 June 2007,.

Hall, D.K. and Riggs, G.A., 2007b, Accuracy assessment of the MODIS snow-cover products. Hydrological Processes, 21:1534-1547.

Hall, D.K., Riggs, G.A. and Foster, F.L., in preparation, New gap-filled MODIS daily snow-cover products.

Hallikainen, M.T., Jääskeläinen, V.S., Pulliainen, J., Koskinen, J., 2000, Transmissivity of Boreal Forest Canopies for Microwave Radiometry of Snow. In *IEEE Transactions on Geoscience and Remote Sensing*, 1564-1566.

Hallikainen, M.T., Halme, P., Takala, M., Pulliainen, J., 2002, Effects of Temperature and Moisture of Snow and Soil on SSM/I Response to Snow. In *IEEE Transactions on Geoscience and Remote Sensing*, 680-682.

Hallikainen M., Halme, P., Lahtinen, P. and Pulliainen, J., 2003, Combined active and passive microwave remote sensing in Finland. In *Proc. of IEEE Geoscience and Remote Sensing Symposium, IGARSS 2003, Toulouse, France*.

Hallikainen M., Halme, P., Lahtinen, P. and Pulliainen, J., 2004, Retrieval of snow characteristics from spaceborne scatterometer data, In *Proc. of IEEE Geoscience and Remote Sensing Symposium, IGARSS 2004, Anchorage, Alaska, USA*, Conference CD.

Hansen, M.C., DeFries, R.S., Townshend, J.R.G., Carroll, M., Dimiceli, C. and Sohlberg, R.A., 2003, Global Percent Tree Cover at a spatial resolution of 500 meters: first results of the MODIS vegetation continuous fields algorithm. *Earth Interactions*, *Volume 7, Issue 10*, pp. 1-15.

Kelly R.E.J., Chang, A.T.C., Tsang, L., and Foster, J.L., 2003, A prototype AMSR-E global snow area and snow depth algorithm. *IEEE Trans. Geosci. Remote Sens.*, EO-1 Special Issue, 41 (2):230-242.

Kelly, R.E.J., in press, The AMSR-E Snow Depth Algorithm: Description and Initial Results. *Journal of the Remote Sensing Society of Japan*.

Key, J.R., Collins, J.B., Fowler, C., and Stone, R.S., 1997, High-latitude surface temperature estimates from thermal satellite data. *Remote Sensing of Environment*, 61:302-309.

Kimball, J.S., McDonald, K.C., Keyser, A.R., Frolking, S. and Running, S.W., 2001, Application of NASA Scatterometer (NSCAT) for determining the daily frozen and nonfrozen landscape of Alaska. *Remote Sensing of Environment*, 75:113-126.

Klein, A.G., Hall, D.K. and Riggs, G.A., 1998, Improving snow-cover mapping in forests through the use of a canopy reflectance model. Hydrological Processes 12:1723-1744.

Klein, A.G. and Stroeve, J., 2002, Development and validation of a snow albelo algorithm for the MODIS instrument. Annals of Glaciology 34: 45-52.

Krenke, A., 1998, updated 2004. Former Soviet Union hydrological snow surveys, 1966-1996. Edited by NSIDC. Boulder, CO, National Snow and Ice Data Center/World Data Center for Glaciology, Digital media.

Matzler, C. and Standley, A., 2000, Relief effects for passive microwave remote sensing. *International Journal of Remote Sensing*, 21, 2403-2412.

Nghiem, S.V., and Tsai, W.Y., 2001a, Global snow cover monitoring with spaceborne Ku-band scatterometer. *IEEE Transactions on Geoscience and Remote Sensing*, 39, 2118-2134.

Nghiem, S.V., Steffen, K., Kwok, R., and Tsai, W.Y., 2001b, Detection of snow melt regions on the Greenland ice sheet using diurnal backscatter change. *Journal of Glaciology*, 47:539-547.

Nghiem S.V., Steffen, K., Neumann, G. and Huff, R., 2005, Mapping ice layer extent and snow accumulation in the percolation zone of the Greenland ice sheet. *Journal of Geophysical Research*, 110, doi:10.1029/2004JF000234.

Ramage, J.M. and Isacks, B.L., 2002, Determination of melt onset and refreeze timing on southeast Alaskan icefields using SSM/I diurnal amplitude variations. Annals of Glaciology, 34:391-398.

Ramage, J.M., Apgar, J.D., McKenney, R.A. and Hannah, W., 2007, Spatial variability of snowmelt timing from AMSR-E and SSNM passive microwave sensors, Pelly River, Yukon Territory, Canada, *Hydrological Processes,* 21: 1548-1560.

Riggs, R.A., Hall, D.K. and Salomonson, V.V., 2006, *MODIS Snow Products User Guide,* available online at http://modis-snow-ice.gsfc.nasa.gov/sugkc2.html.

Salomonson, V.V. and Appel, I., 2004, Estimating the fractional snow covering using the normalized difference snow index. *Remote Sensing of Environment*, 89:351-360.

Schmugge, T., 1980, Techniques and applications of microwave radiometry, in *Remote Sensing in Geology*, Siegal, B.S. and Gillespie, A.R. (eds), John Wiley, New York, Chapter 11, 337-352.

Sturm, M., Holmgren, J. and Liston, G.E., 1995, A seasonal snow cover classification system for local to regional applications. *Journal of Climate*, 8, 1261-1283.

Tedesco, M., Kim, E.J., Gasiewski, A. and Stankov, B., 2005, Analysis of multi-scale radiometric data collected during the Cold Land Processes Experiment -1 (CLPX-1), *Geophysical Research Letters*, 32, L18501.

Tedesco, M., 2007, Snowmelt detection over the Greenland ice sheet from SSM/I brightness temperature daily variations, *Geophysical Research Letters*., 34, L02504,doi:10.1029/2006GL028466.

Walker, A.E. and B. Goodison, B., 2000, Challenges in determining snow water equivalent over Canada using microwave radiometry, *Proceedings of IGARSS 2000, Honolulu, HI*, 24-28 July 2000.

List of Tables:

List of Figures:

Figure 11: AMSR-E SWE and snow course SWE histogram comparison at the Sodankylä stations for November 2006 – March 2007.

Table 1

Band number	Bandwidth (μm)	Used in snow algorithms and Terra and/or Aqua Satellites
1	0.62-0.67	Terra & Aqua
2	0.841-0.876	Terra & Aqua
4	0.545-0.565	Terra & Aqua
6	1.628-1.672	Terra
7	2.105-2.155	Aqua
31	10.780-11.280	Terra & Aqua
32	11.770-12.270	Terra & Aqua

Table 2

Long Name	Earth Science Data Type (ESDT)	Spatial Resolution
MODIS/Terra Snow Cover 5-Min L2 Swath 500m*	MOD10_L2	500-m resolution, swath of MODIS data
MODIS/Terra Snow Cover Daily L3 Global 500m SIN Grid (includes daily snow albedo)	MOD10A1	500-m resolution, projected, gridded tile data
MODIS/Terra Snow Cover 8-Day L3 Global 500m SIN Grid	MOD10A2	500-m resolution, projected, gridded tile data
MODIS/Terra Snow Cover Daily L3 Global 0.05Deg CMG	MOD10C1	0.05° resolution, lat/lon climate modeling grid
MODIS/Terra Snow Cover 8-Day L3 Global 0.05Deg CMG	MOD10C2	0.05° resolution, lat/lon climate modeling grid
MODIS/Terra Snow Cover Monthly L3 Global 0.05Deg CMG**	MOD10CM	0.05° resolution, lat/lon climate modeling grid
MODIS/Aqua Snow Cover 5-Min L2 Swath 500m*	MYD10_L2	500-m resolution, swath of MODIS data
MODIS/Aqua Snow Cover Daily L3 Global 500m SIN Grid (includes daily snow albedo)	MYD10A1	500-m resolution, projected, gridded tile data
MODIS/Aqua Snow Cover 8-Day L3 Global 500m SIN Grid	MYD10A2	500-m resolution, projected, gridded tile data
MODIS/Aqua Snow Cover Daily L3 Global 0.05Deg CMG	MYD10C1	0.05° resolution, lat/lon climate modeling grid
MODIS/Aqua Snow Cover 8-Day L3 Global 0.05Deg CMG	MYD10C2	0.05° resolution, lat/lon climate modeling grid
MODIS/Aqua Snow Cover Mmonthly L3 Global 0.05Deg CMG **	MYD10CM	0.05° resolution, lat/lon climate modeling grid
*A FSC enhancement at 500-m resolution will be available in 2004.		
**Future enhancement (see text for explanation).		

Table 3

	SMMR	SSM/I	AMSR-E
Platform	Nimbus-7	DMSP F-8, 11, 13	Aqua
Period of Operation	1979-87	1987-present	2002-present
Data Acquisition	every other day	daily	daily
Swath Width	780 km	1400 km	1600 km
Frequency (GHz)	18.0 37.0	19.35 37.0	18.7 36.5
Spatial Resolution (km)	60x40	69x43	28x16
	(18GHz)	(19.4 GHz)	(19.7 GHz)
	30x20	37x29	14x8
	(37 GHz)	(37 GHz)	(36.5 GHz)
Polarization	H & V	H & V	H & V
Orbital Timing (Eq. Crossing)	Midnight	6:00 a.m.	1:30 a.m.
(for minimum temperature)			
Incidence angle	51	53	53

Table 4

Station ID (LPNN)	Station Name	Latitude (N)	Longitude (E)	Elevation (m)
8405	Kittilä Tepsa	67°33′	25°41′	205
7707	Savukoski Värriö	67°28′	28°00′	220
7501	Sodankylä	67°22′	26°37′	179
6707	Taivalkoski Paloasema	65°34′	28°14′	203
6704	Taivalkoski Inget	65°44′	28°33′	248
6702	Kuusamo Maanselkä Kurkijärvi	65°56′	28°58′	310
4506	Pyhäjärvi Ol Lohvanperä	63°46′	26°05′	160
4407	Kärsämäki Venetpalo	63°53′	25°47′	120
4405	Haapajärvi Välioja Nokkous	63°45′	25°28′	130

Figure 1

ANSA snow map 15 January 2007

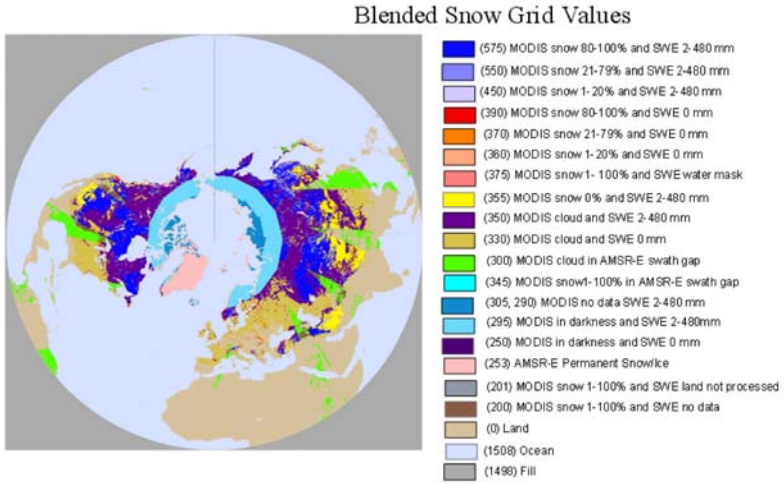

ANSA snow map 15 January 2007

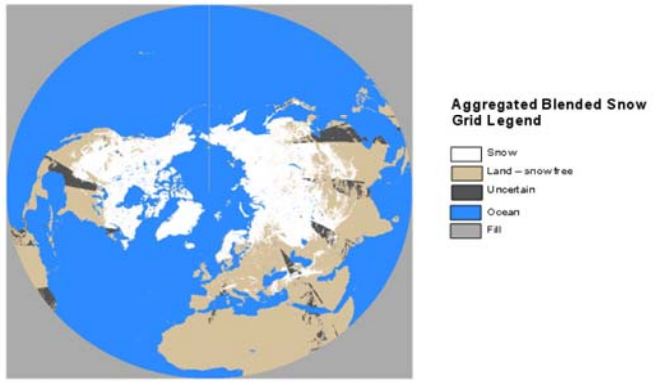

Figure 2

ANSA snow map 15 February 2007

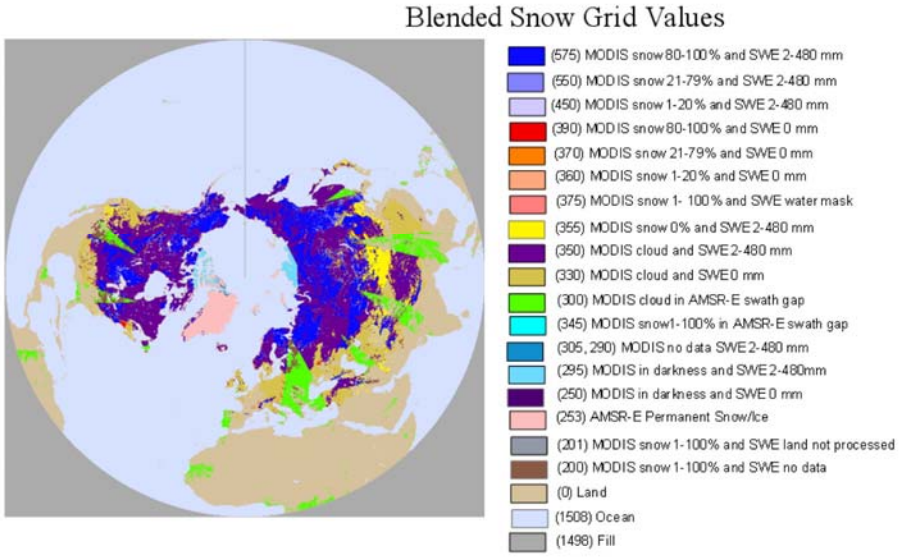

ANSA snow map 15 February 2007

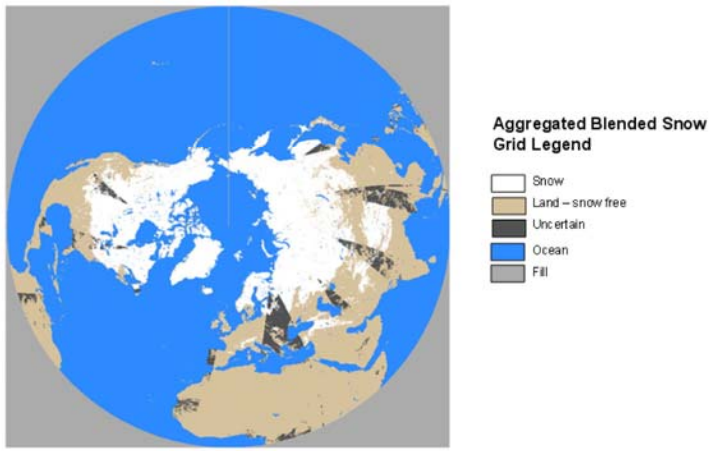

Figure 3

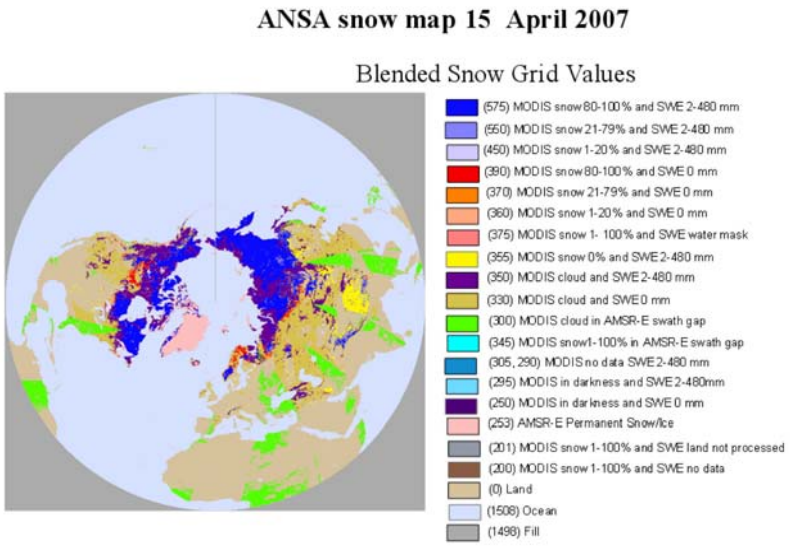
ANSA snow map 15 April 2007
Blended Snow Grid Values
(575) MODIS snow 80-100% and SWE 2-480 mm
(550) MODIS snow 21-79% and SWE 2-480 mm
(450) MODIS snow 1-20% and SWE 2-480 mm
(390) MODIS snow 80-100% and SWE 0 mm
(370) MODIS snow 21-79% and SWE 0 mm
(360) MODIS snow 1-20% and SWE 0 mm
(375) MODIS snow 1- 100% and SWE water mask
(355) MODIS snow 0% and SWE 2-480 mm
(350) MODIS cloud and SWE 2-480 mm
(330) MODIS cloud and SWE 0 mm
(300) MODIS cloud in AMSR-E swath gap
(345) MODIS snow1-100% in AMSR-E swath gap
(305, 290) MODIS no data SWE 2-480 mm
(295) MODIS in darkness and SWE 2-480mm
(250) MODIS in darkness and SWE 0 mm
(253) AMSR-E Permanent Snow/Ice
(201) MODIS snow 1-100% and SWE land not processed
(200) MODIS snow 1-100% and SWE no data
(0) Land
(1508) Ocean
(1498) Fill

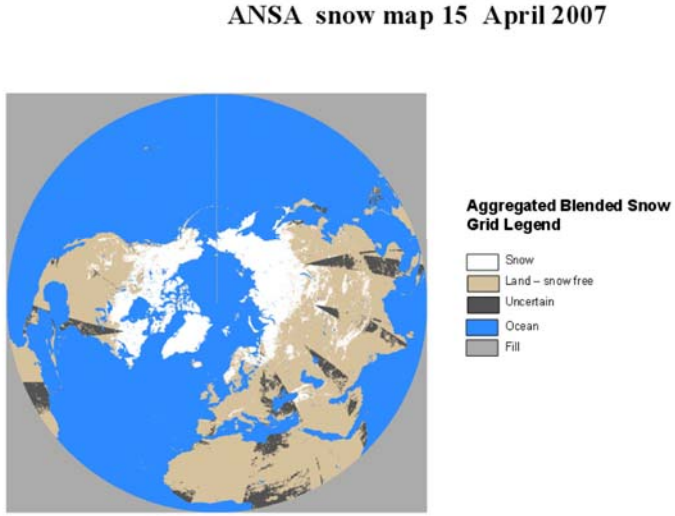
ANSA snow map 15 April 2007
Aggregated Blended Snow Grid Legend
Snow
Land – snow free
Uncertain
Ocean
Fill

Figure 4

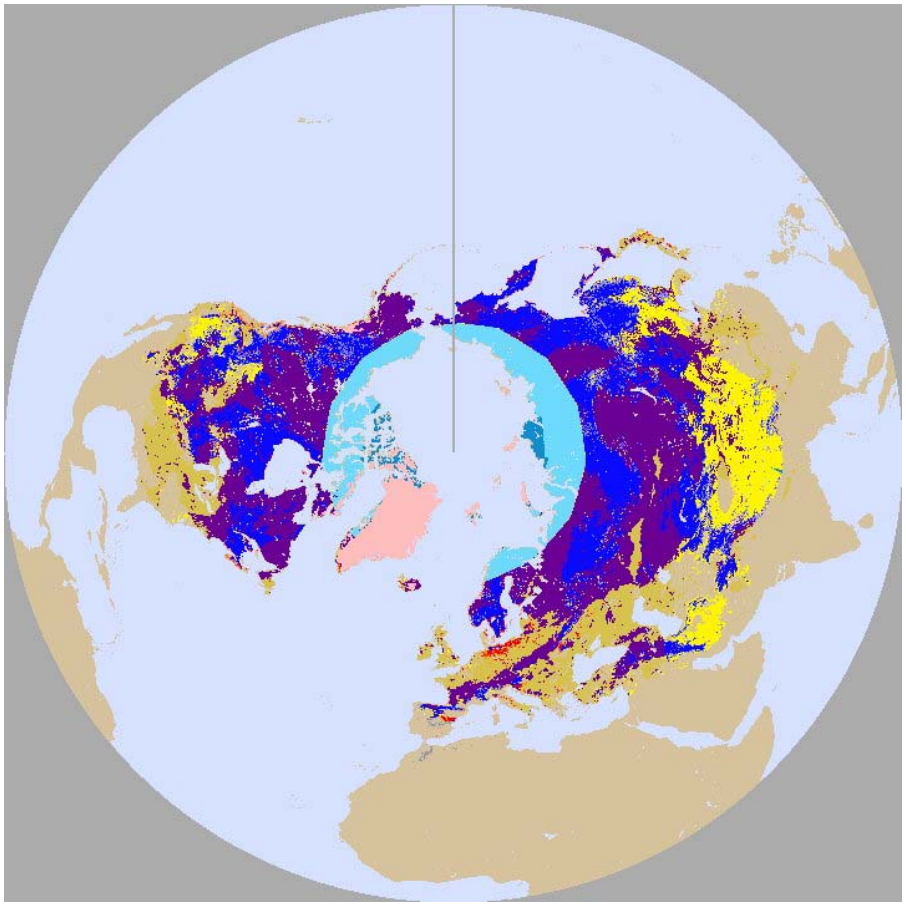

Figure 5

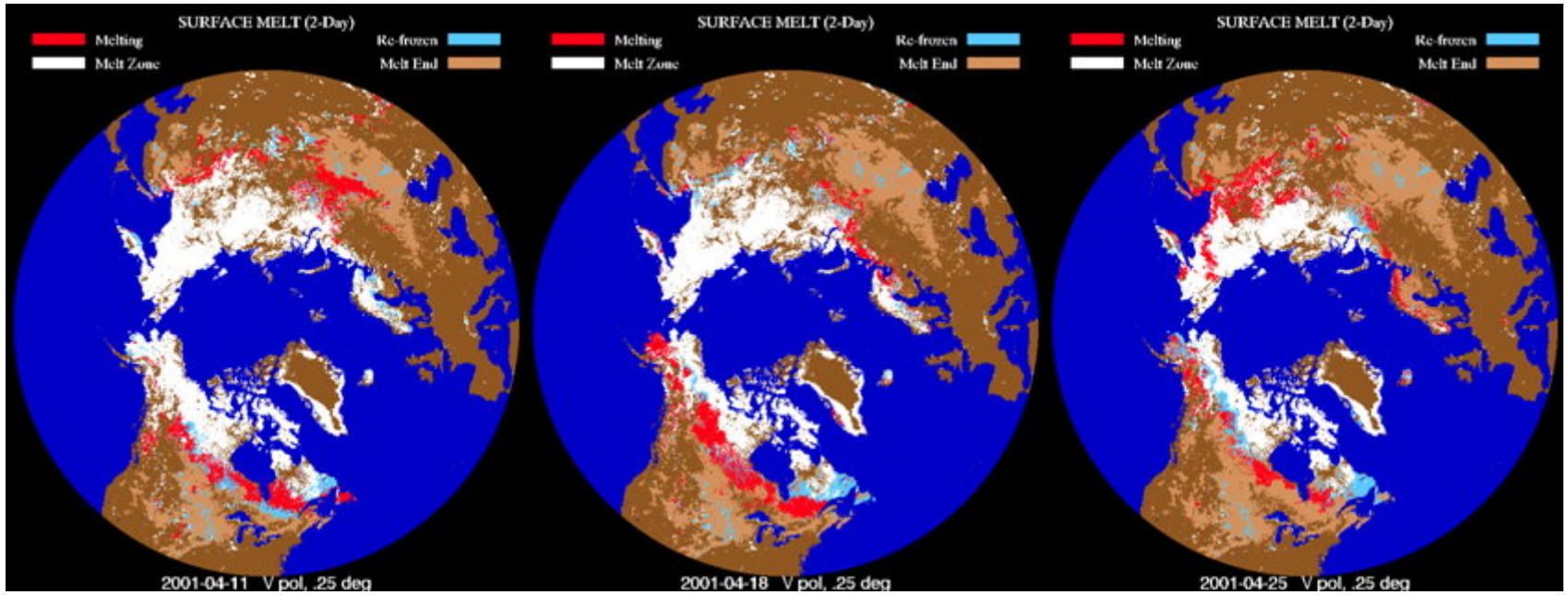
SURFACE MELT (2-Day)
Melting
Melt Zone
Re-frozen
Melt End
2001-04-11 V pol, .25 deg
SURFACE MELT (2-Day)
Melting
Melt Zone
Re-frozen
Melt End
2001-04-18 V pol, .25 deg
SURFACE MELT (2-Day)
Melting
Melt Zone
Re-frozen
Melt End
2001-04-25 V pol, .25 deg

Figure 6

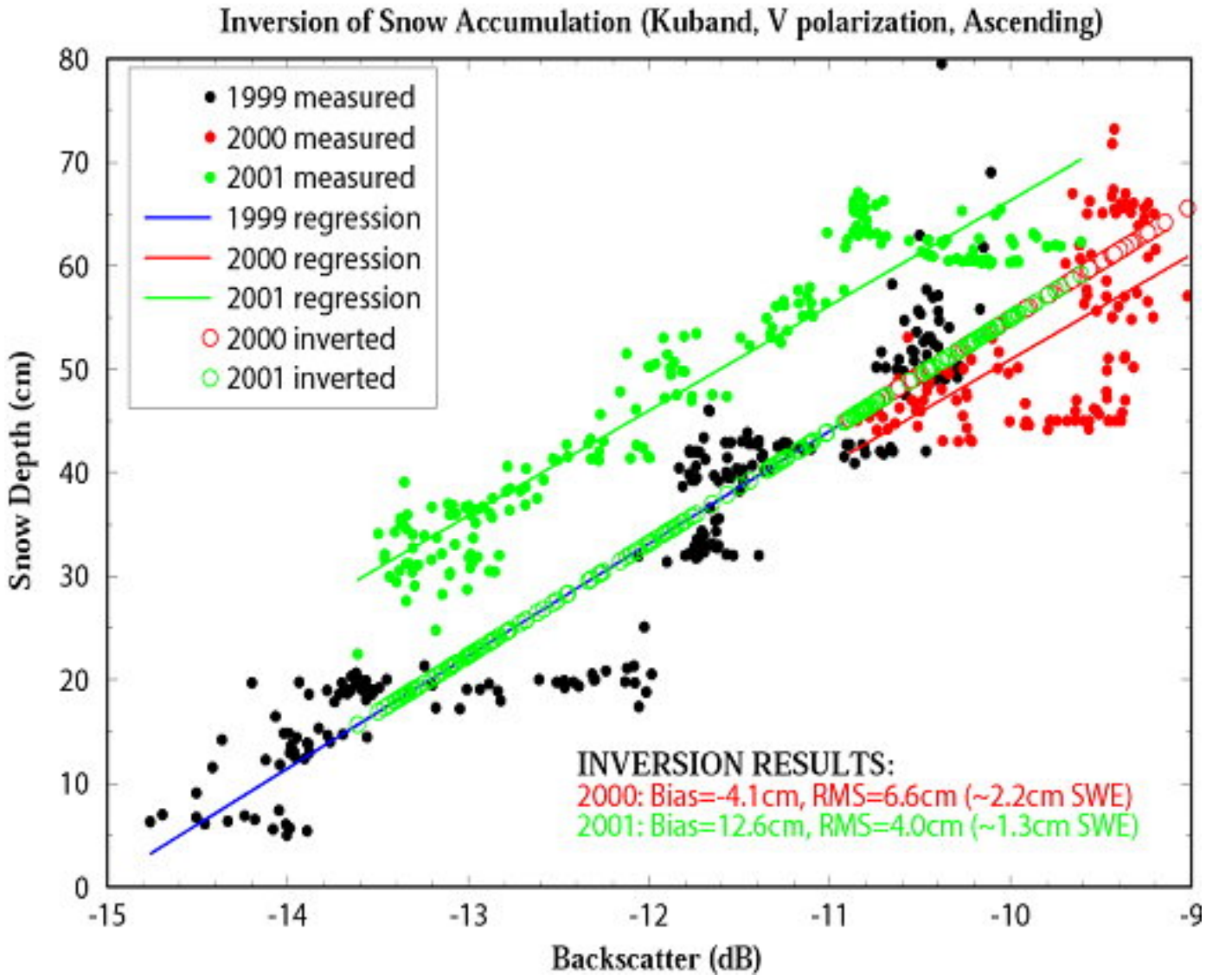
Inversion of Snow Accumulation (Kuband, V polarization, Ascending)
1999 measured
2000 measured
2001 measured
1999 regression
2000 regression
2001 regression
2000 inverted
2001 inverted
INVERSION RESULTS:
2000: Bias=-4.1cm, RMS=6.6cm (~2.2cm SWE)
2001: Bias=12.6cm, RMS=4.0cm (~1.3cm SWE)
Snow Depth (cm)
Backscatter (dB)
0
10
20
30
40
50
60
70
80
-15
-14
-13
-12
-11
-10
-9

Figure 7

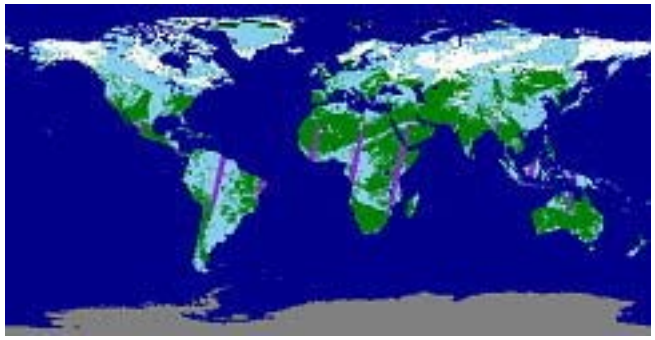

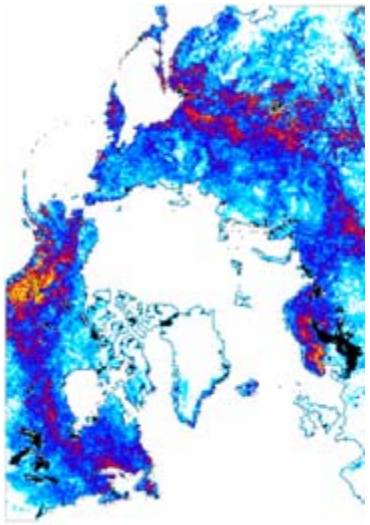

Figure 8

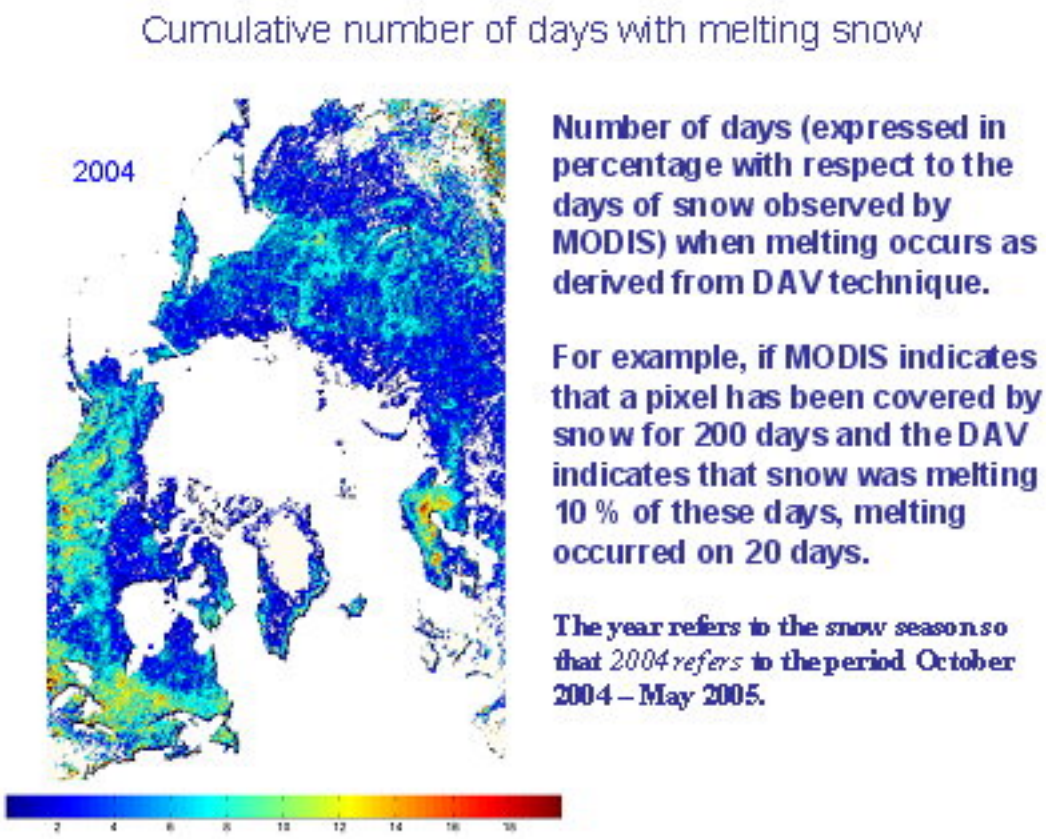
Cumulative number of days with melting snow
2004
Number of days (expressed in percentage with respect to the days of snow observed by MODIS) when melting occurs as derived from DAV technique.
For example, if MODIS indicates that a pixel has been covered by snow for 200 days and the DAV indicates that snow was melting 10 % of these days, melting occurred on 20 days.
The year refers to the snow season so that 2004 refers to the period October 2004 – May 2005.

Figure 9

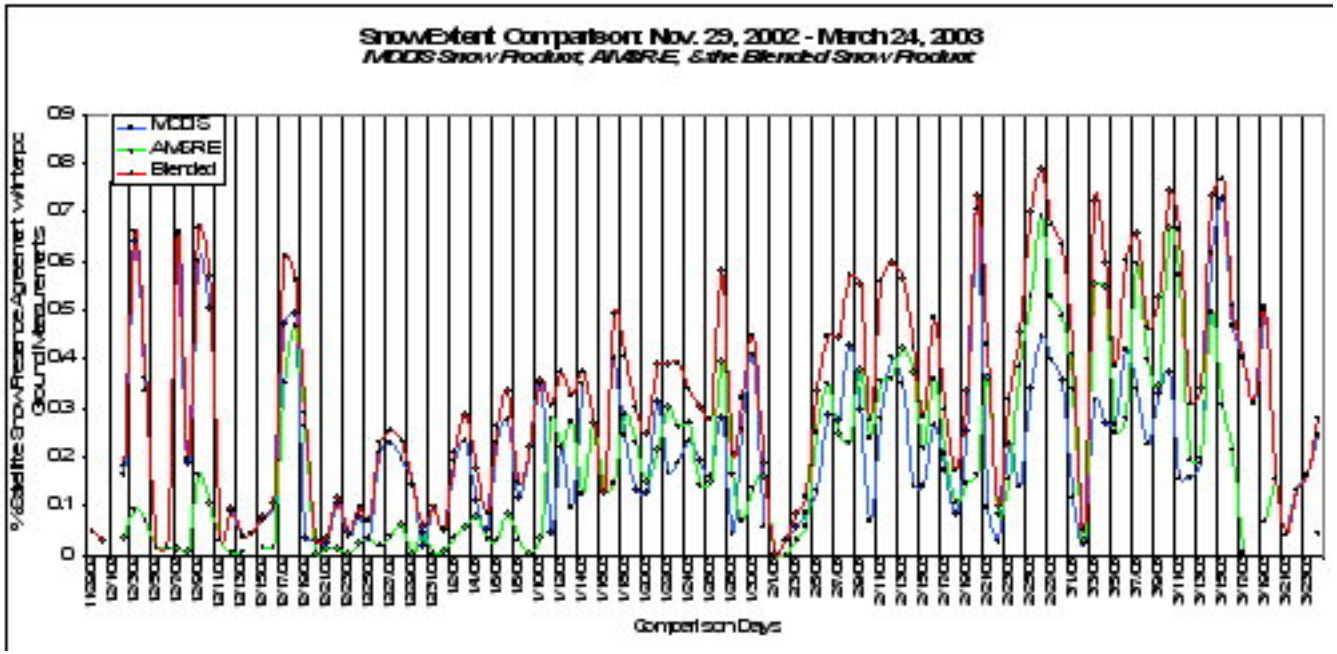
Snow Extent Comparison Nov. 29, 2002 - March 24, 2003
MODIS Snow Product, AMSR-E, & the Blended Snow Product
MODIS
AMSRE
Blended
Comparison Days

Figure 10

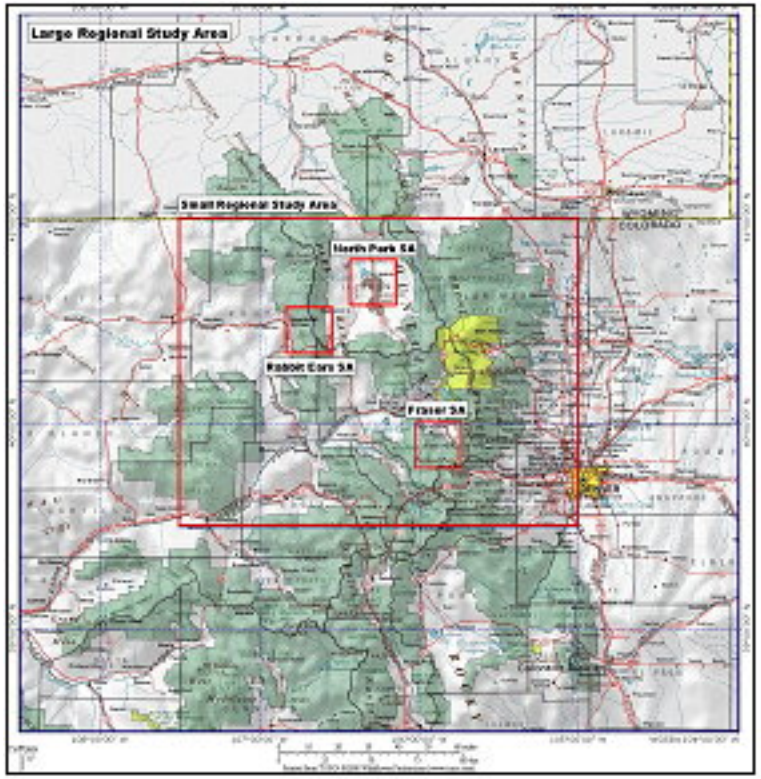

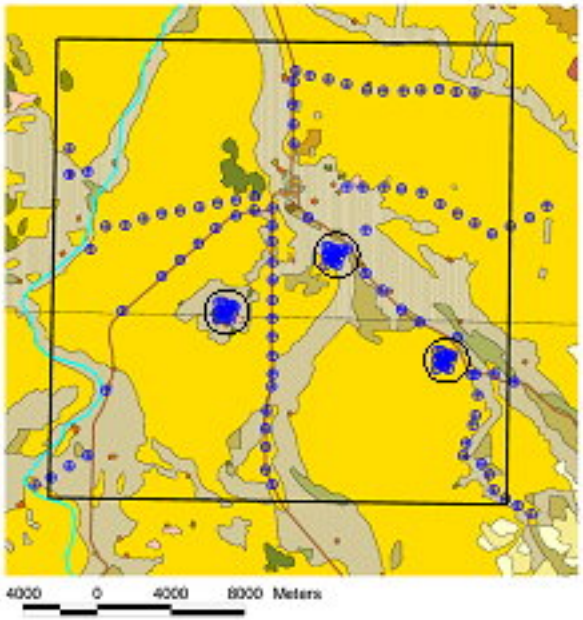

Figure 10a

Figure 10b

Figure 11

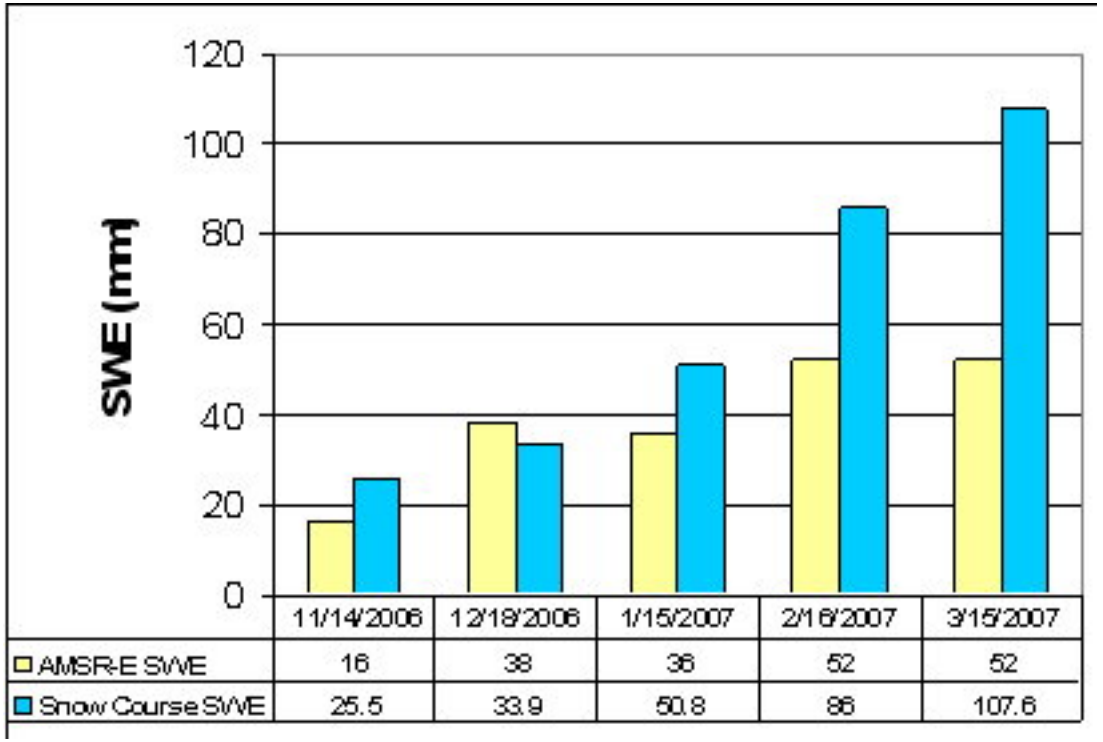

	11/14/2006	12/18/2006	1/15/2007	2/16/2007	3/15/2007
AMSR-E SWE	16	38	36	52	52
Snow Course SWE	25.5	33.9	50.8	86	107.6